Perturbation-response analysis of *in silico* metabolic dynamics: Hard-coded responsiveness in the cofactors and network sparsity

Yusuke Himeoka[a,1] **and Chikara Furusawa**[a,b]

[a]Universal Biology Institute, University of Tokyo, 7-3-1 Hongo, Bunkyo-ku, Tokyo, Japan; [b]Center for Biosystem Dynamics Research, RIKEN, 6-2-3 Furuedai, Suita, Osaka, Japan

This manuscript was compiled on October 30, 2023

Homeostasis is a fundamental characteristic of living systems. Unlike rigidity, homeostasis necessitates that systems respond flexibly to diverse environments. Understanding the dynamics of biochemical systems when subjected to perturbations is essential for the development of a quantitative theory of homeostasis. In this study, we analyze the response of bacterial metabolism to externally imposed perturbations using kinetic models of *Escherichia coli*'s central carbon metabolism. We found that three distinct kinetic models consistently display strong responses to perturbations; In the strong responses, minor initial discrepancies in metabolite concentrations from steady-state values amplify over time, resulting in significant deviations. This pronounced responsiveness is a characteristic feature of metabolic dynamics, especially since such strong responses are seldom seen in toy models of the metabolic network. Subsequent numerical studies show that adenyl cofactors consistently influence the responsiveness of the metabolic systems across models. Additionally, we examine the impact of network structure on metabolic dynamics, demonstrating that as the metabolic network becomes denser, the perturbation response diminishes—a trend observed commonly in the models. To confirm the significance of cofactors and network structure, we constructed a simplified metabolic network model, underscoring their importance. By identifying the structural determinants of responsiveness, our findings offer implications for bacterial physiology, the evolution of metabolic networks, and the design principles for robust artificial metabolism in synthetic biology and bioengineering.

metabolism | microbiology | dynamical systems

For bacterial cells growing under fixed, substrate-rich culture conditions, several quantitative laws pertaining to the physiology of growing bacteria have been identified. These include the linear association between growth rate and the ribosomal fraction in total proteomes (1, 2), the linear relationship linking substrate uptake to growth rate (3), and the correlations between transcriptional responses to various sublethal stresses (4).

The physiological state of continuously growing bacteria is believed to approximate a steady state. Owing to this steadiness, these experimental laws have been theoretically rationalized (2, 4–7). Moreover, theoretical tools have been developed to predict cellular metabolic states. One of the most successful of these tools is Flux Balance Analysis, which significantly reduces the data required compared to other modeling methods by leveraging the steady-state assumption of the metabolic state (8, 9).

In recent years, the physiology of bacteria during out-of-steady growth has garnered significant attention. A wealth of intriguing phenomena under such conditions has been gradually revealed. For instance, cells can "remember" the duration of starvation and the nature of environmental changes—such as the rate at which nutrients deplete—and this can dramatically alter the distribution of lag times (10–13). Both the proteome and metabolome of starved cells display characteristically slow dynamics (14). The metabolites used for storage play a pivotal role in fluctuating environments (15). Further, there is a trade-off between the growth rate under nutrient-rich conditions and other physiological parameters: namely, the lag time upon nutrient shifts (16) and the death rate under starved conditions (17).

For a comprehensive understanding of bacterial physiology during out-of-steady growth—which three of the four classical bacterial growth phases (18)—it is essential to develop quantitative theories that describe the dynamics of cellular physiology in tandem with experimental approaches. Given the inherent dynamic behavior, constraint-based modeling approaches like Flux Balance Analysis fall short in capturing the phenomena mentioned earlier, primarily because they assume that the intracellular state is in a steady state. Dynamic perspectives on bacterial physiology are thus indispensable.

In contrast to this need, quantitative theories addressing the dynamics of bacterial physiology remain underdeveloped. A comprehensive understanding of bacterial physiology under extreme conditions, such as temporally varying or highly stressful environments where cells struggle to survive, remains

DRAFT

Significance Statement

Understanding the dynamics of metabolic systems is vital for deciphering cellular functions and their responses to environmental shifts. However, the advancement of dynamic theories for cellular metabolism lags behind its static counterparts. In this study, we delve into the dynamic responses of *Escherichia coli*'s central carbon metabolism to perturbations. We found that the response of the cellular metabolism is stronger than that of the random network-based metabolic models. Also, our results highlight the critical role of adenyl cofactor dynamics, such as ATP, and sparse network structure in dictating response strength. These findings carry profound implications across bacterial physiology, evolutionary biology, and synthetic biology.

Author contributions: Y.H and C.F designed research; Y.H performed research; Y.H analyzed data; and Y.H and C.F wrote the paper.

The authors declare no competing interest.

[1] To whom correspondence should be addressed. E-mail:yhimeoka@g.ecc.u-tokyo.ac.jp

elusive. As a foundational step in theory-building, we delve into understanding how the metabolic system reacts when metabolic states deviate from the steady state. Systems' responses to perturbations are often studied as an initial step for the explorations of systems' dynamic properties beyond the steady state (19, 20).

In this manuscript, we examine the kinetic models of *Escherichia coli*'s central carbon metabolism and ask how the metabolic state responds to perturbations. We study three independently proposed kinetic models (21–23), and explore the features shared among the models. We demonstrate that the three models exhibit strong responses to perturbations on the metabolic states; The effects of these perturbations are magnified, leading to significant deviations in metabolite concentrations from their steady-state values, depending on which and how metabolite concentrations are perturbed. The observed responsiveness is a hallmark of the realistic metabolic network as the toy metabolic models lack such a strong response. Computational analysis revealed that cofactors, such as ATP and ADP, play a crucial role in the strong response to perturbations. We also discovered the importance of the sparse structure of the metabolic network by adding virtual reactions to it. To validate our findings, we developed a simple, minimal model of metabolic reactions, and we confirmed that cofactor dynamics and network sparsity are indeed the key ingredients of the strong responses.

Results

Model. In the present study, we investigate the dynamic response of metabolic states to perturbations in metabolite concentrations using kinetic models of *E.coli* central carbon metabolism. In kinetic modeling approaches, the temporal evolution of metabolites' concentrations is modeled using ordinary differential equations to capture behaviors in out-of-steady-state metabolism.

We employ three kinetic models of *E.coli*'s central carbon metabolism, emphasizing the common features exhibited by the models. A limitation of kinetic models is their specificity; unlike constraint-based modeling, kinetic modeling necessitates extensive biochemical information, such as the function form of the reaction rate equation and the parameter values for each reaction. By examining a single kinetic model, conclusions may apply only to that specific model. Therefore, our focus lies on the shared features of the three models to circumvent the limitations of individual model specificity. We also believe there is potential for the results obtained commonly among the models to apply to real biological systems as well.

The models under consideration are those proposed by Chassagnole et al. (21), Khodayari et al. (22), and Boecker et al. (23). While all three models incorporate the glycolytic pathway, only the models by Khodayari et. al. and Chassagnole et. al. feature the pentose phosphate (PP) pathway. Notably, the Chassagnole model excludes the tricarboxylic acid (TCA) cycle. A graphical summary of the metabolic modules in these models is presented in Fig. 1A.

The Boecker and Chassagnole models utilize glucose as the sole carbon source, whereas the Khodayari model can assimilate other carbon sources, such as fructose, formate, and acetate depending on differences between the extracellular- and intracellular concentrations. The Boecker model explicitly models biomass formation, considering several metabolites as biomass precursors that are consumed with a fixed stoichiometry to produce biomass. Conversely, the Khodayari and Chassagnole models do not incorporate the biomass formation reaction. Instead, biomass precursor metabolites are consumed independently, implying that the stoichiometry of biomass formation varies depending on the concentrations. The dilution effect due to the volume growth is modeled in both the Boecker and Chassagnole models. In the Boecker model, the dilution rate corresponds proportionally to the biomass formation reaction rate, while it remains constant in the Chassagnole model. The Khodayari model omits the dilution effect. In addition to the metabolic reaction implemented in each model, the specific forms of the reaction rate equations also differ among the models.

Within these models, the dynamics of gene regulation mediated by transcription factors are not modeled; that is, the total concentration of each metabolic enzyme is constant allosteric regulations are incorporated into the models (for a detailed description, see *Materials and Methods*).

Perturbation-response simulation. In this section, we present the results of a series of simulations, which we call perturbation-response simulations. These simulations highlight the unique responses of the metabolic models to perturbations and shed light on the dynamic behavior of metabolic systems. It may be useful for the reader to first describe the perturbation-response simulation procedure. The procedure is consistently applied across all three models used in our study and can be summarized as follows:

1. Compute the growing steady-state attractor.
2. Generate N_{ini} initial points by perturbing the metabolite concentrations from the attractor.
3. Simulate the model dynamics starting from each initial point.

1. Computing the attractor. First, we identify the steady-state attractor where the production/consumption of each metabolite is balanced. For the Khodayari and Boecker models, the attractor corresponds to the steady-state studied in their original papers. For the Chassagnole model, we numerically determined the steady-state attractor (details provided in *Materials and Methods*).

2.Generating the initial points by perturbation. Once the steady-state attractor has been computed, we establish a set of initial points for subsequent computations by perturbing the metabolite concentrations. This perturbation is a proxy for stochastic fluctuations within cells. We postulate that the perturbation source is the variability in protein concentrations due to the inherent randomness of transcription and translation processes. Based on a stochastic model of transcription and translation with a biologically relevant setup, the relative size of the concentration fluctuations is estimated to be several tens of percent (for a detailed derivation, see *Materials and Methods*). Consequently, the perturbed concentration of chemical n as $x_n = r_n x_n^{\mathrm{st}}$, where r_n is a uniformly distributed random number with a maximum strength of 40%, i.e. ranging from 0.6 to 1.4. The choice of uniform distribution is not essential for the following result. Also, the characteristic features of the response studied later remain consistent even when different perturbation strengths are employed (see Fig. S1).

DRAFT

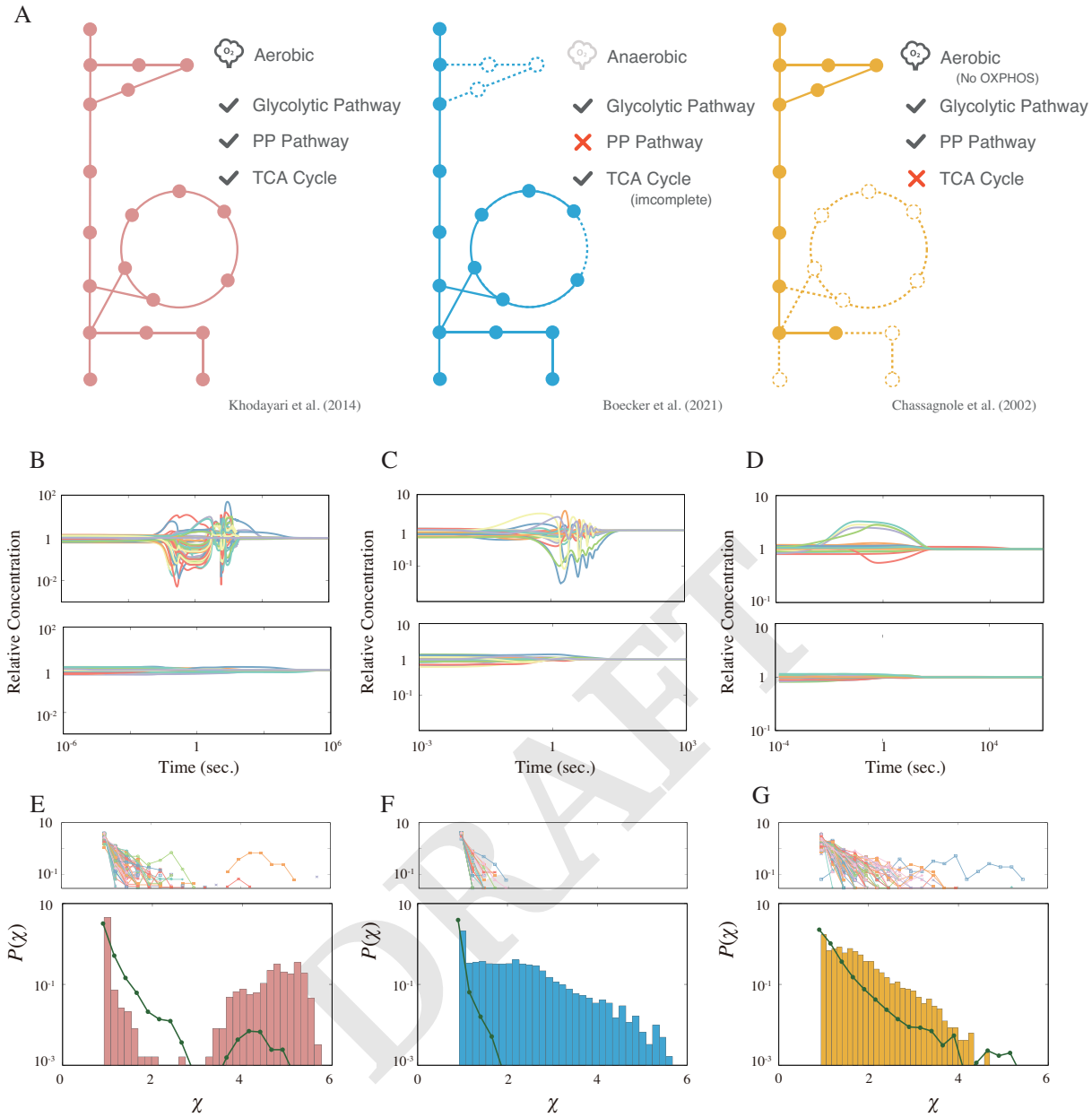

Fig. 1. (A). A graphical summary of the three models used in this study. The solid circles represent the metabolites and the lines represent the metabolic reactions. The dashed circles and lines are the subsystems not implemented in the model. (B-D). Example time courses for each model. The top and bottom panels are examples of the strong and weak response, respectively. (E-G). The response coefficient distribution $P(\chi)$ of each model (bottom). The average response coefficient distribution of the random catalytic reaction network (RCRN) model is overlaid (green line). The response coefficient distribution of each instance of the RCRN model is shown on the top panel. The model schemes, time courses, and distributions are aligned in each column, i.e. the leftmost network of (A), (B), and (E) are from the model developed by Khodayari et al. (22).

3.Simulating the dynamics. We compute the model dynamics using the N_{ini} points generated by the perturbation as initial points to explore the metabolic response to the perturbations. As far as we have tried, all initial points have returned to the original growing steady state, and thus, we hereafter study the relaxation behavior.

Strong responses in the kinetic models. After executing the perturbation-response simulations for the models, we observed distinct relaxation dynamics in each. In Fig. 1B-D, the top and bottom panels display typical examples of dynamics from each model that either respond strongly or weakly to perturbations. In the weakly responding dynamics (bottom panel), the effects of the perturbations diminish almost monotonically. Conversely, in the dynamics that respond strongly (top panel), the initial displacements of concentrations are amplified over time, leading some metabolites' concentrations to overshoot or undershoot (significant concentration changes in metabolites are highlighted in Fig.S2).

For more in-depth analysis, we introduce a measure of the

responsiveness to the perturbation that we call the response coefficient χ, defined as

$$\chi = \max_t \frac{\| \ln \boldsymbol{x}(t) - \ln \boldsymbol{x}^{\mathrm{st}} \|}{\| \ln \boldsymbol{x}(0) - \ln \boldsymbol{x}^{\mathrm{st}} \|},$$

where $\| \cdot \|$ is the Euclidean norm. The response coefficient distributions for each model are plotted in the bottom panels of Fig. 1E-G. All three models have the peak at $\chi = 1$ (note that this is the minimum value of χ). These peaks correspond to the trajectories where the Euclidean distance between the state and the attractor decreases monotonically with time (i.e. $\max_t \| \ln \boldsymbol{x}(t) - \ln \boldsymbol{x}^{\mathrm{st}} \| = \| \ln \boldsymbol{x}(0) - \ln \boldsymbol{x}^{\mathrm{st}} \|$). In addition, the distribution of the Khodayari model exhibits another peak in a larger χ region while the other two models have plateaus adjacent to the primary peak.

For comparison purposes, we conducted perturbation-response simulations for the random catalytic reaction networks (RCRN) model, a toy model of the metabolic network (24, 25). In one instance of the RCRN model, the "metabolites" are interconnected through a random network, and every metabolite is considered a catalyst as well as a reactant. We generated 128 instances of the RCRN model, each having the same number of metabolites and the same distribution of the reaction rate constant. For instance, to draw a comparison with the Khodayari model, we generated the model instances with 778 metabolites and 3112 reactions, where the reaction rate constants are randomly chosen from that of the Khodayari model (detailed construction of the RCRN model is provided in *Materials and Methods*). The top panel of Fig. 1E-G presents the response coefficient distribution for each RCRN model instance, represented by different lines. Additionally, the "average" response coefficient distribution, which is the mean of the distributions plotted in the top panel, is overlaid (green dotted line). As a fact, the emergence of the additional peak and plateaus, indicative of strong responsiveness, are unique traits of the realistic metabolic reaction network model and are seldom seen in toy representations of the metabolic network.

Key metabolites on the responsiveness. What factors contribute to the strong responses of the metabolic state? In this section, we investigate which metabolites play pivotal roles in inducing these strong responses in the model. To understand the role of each metabolite's dynamics, we conducted perturbation-response simulations using model equations derived by fixing each metabolite's concentration to its steady-state value. The impact of holding each metabolite's concentration constant is quantified by the change in the average response coefficient:

$$\rho_x^+ = \frac{\langle \chi_x \rangle - \langle \chi_{\mathrm{ori}} \rangle}{\langle \chi_{\mathrm{ori}} \rangle}, \ \left(\langle \chi_x \rangle \geq \langle \chi_{\mathrm{ori}} \rangle \right) \quad [1]$$

$$\rho_x^- = \frac{\langle \chi_{\mathrm{ori}} \rangle - \langle \chi_x \rangle}{\langle \chi_{\mathrm{ori}} \rangle}, \ \left(\langle \chi_x \rangle \leq \langle \chi_{\mathrm{ori}} \rangle \right) \quad [2]$$

where x denotes the metabolites' IDs and χ_x represents the response coefficient of the model with the concentration of the metabolite x fixed to constant. Note that for each metabolite in each model, either the ρ_x^+ or ρ_x^- is defined, depending on whether the modified model (with the metabolite x as a held constant) exhibits an average response coefficient larger (for ρ_x^+) or smaller (for ρ_x^-) than the original model.

Fig. 2 displays $\rho_x^{\pm}$ values for representative metabolites (comprehensive results for all metabolites can be found in Fig. S3). While most metabolites have a bilateral effect on the average response coefficient depending on the original model (or exert a small unilateral effect), ATP and ADP (we refer to them collectively as AXPs) consistently demonstrate a marked impact in reducing the average response coefficient across models. This observed significance of AXPs in metabolic dynamics aligns with previous findings (26).

Interestingly, halting the dynamics of several metabolites can amplify the model's response coefficient. Across the models, metabolites that augment the response coefficient when their concentrations are fixed tend to be allosteric regulators associated with negative regulation. Freezing these metabolites' concentrations effectively removes the negative feedback loop present in the metabolic systems. Typically, negative feedback stabilizes system behavior. In the present context, it assists the system in returning to its original state after perturbations. Hence, fixing these metabolites' concentrations allows the system to respond more vigorously to perturbations compared to the original model.

Pyruvate is an exception to the above description, which is not the allosteric regulator in the models. The strong influence of pyruvate on the increase in response coefficients is attributed to the phosphotransferase system (PTS). The external glucose is taken up by converting phosphoenolpyruvate into pyruvate through the PTS. This reaction elevates pyruvate concentration, subsequently decelerating glucose uptake. By holding pyruvate concentration constant, this negative feedback effect is negated, enhancing the autocatalytic nature of the reaction system formed by the PTS and glycolysis ($\mathrm{GLC_{ex}} + \mathrm{PEP} \rightarrow \cdots \rightarrow 2\mathrm{PEP}$).

The role of the sparsity of the networks. The key role of AXPs in changing the kinetic models' responsiveness was shown in the previous section. Nevertheless, this does not imply that all kinetic models of chemical reaction systems with cofactors such as AXPs always exhibit a strong response to perturbations. The strong responses demonstrated by the three models (as seen in Fig. 1B-D) are absent in abstract toy models of metabolism, which consist of random reaction networks incorporating such cofactor chemicals (27). This discrepancy prompts us to investigate other potential determinants causing metabolic models to display strong responses shown in the three models.

A noteworthy attribute of metabolic networks is their inherent sparsity. While cofactors are linked to numerous reactions, the backbone networks—networks excluding cofactors—are distinctly sparse. As an example, the glycolytic pathway predominantly mirrors a linear sequence of reactions, resulting in many metabolites within this pathway participating in merely two reactions.

Does network structure play a role in the dynamics of metabolic systems? For this question, previous research in the opposite direction—reaction dynamics on dense networks—provides useful insights. There are several studies using the random networks as an abstract model of metabolic networks (4, 24, 28, 29). In such types of models, the effect of the initial perturbations on metabolite concentrations typically decays monotonically over time (28, 29). This is in stark contrast to the behavior observed in Fig. 1B-D.

Considering the inherent tendency of random reaction net-

DRAFT

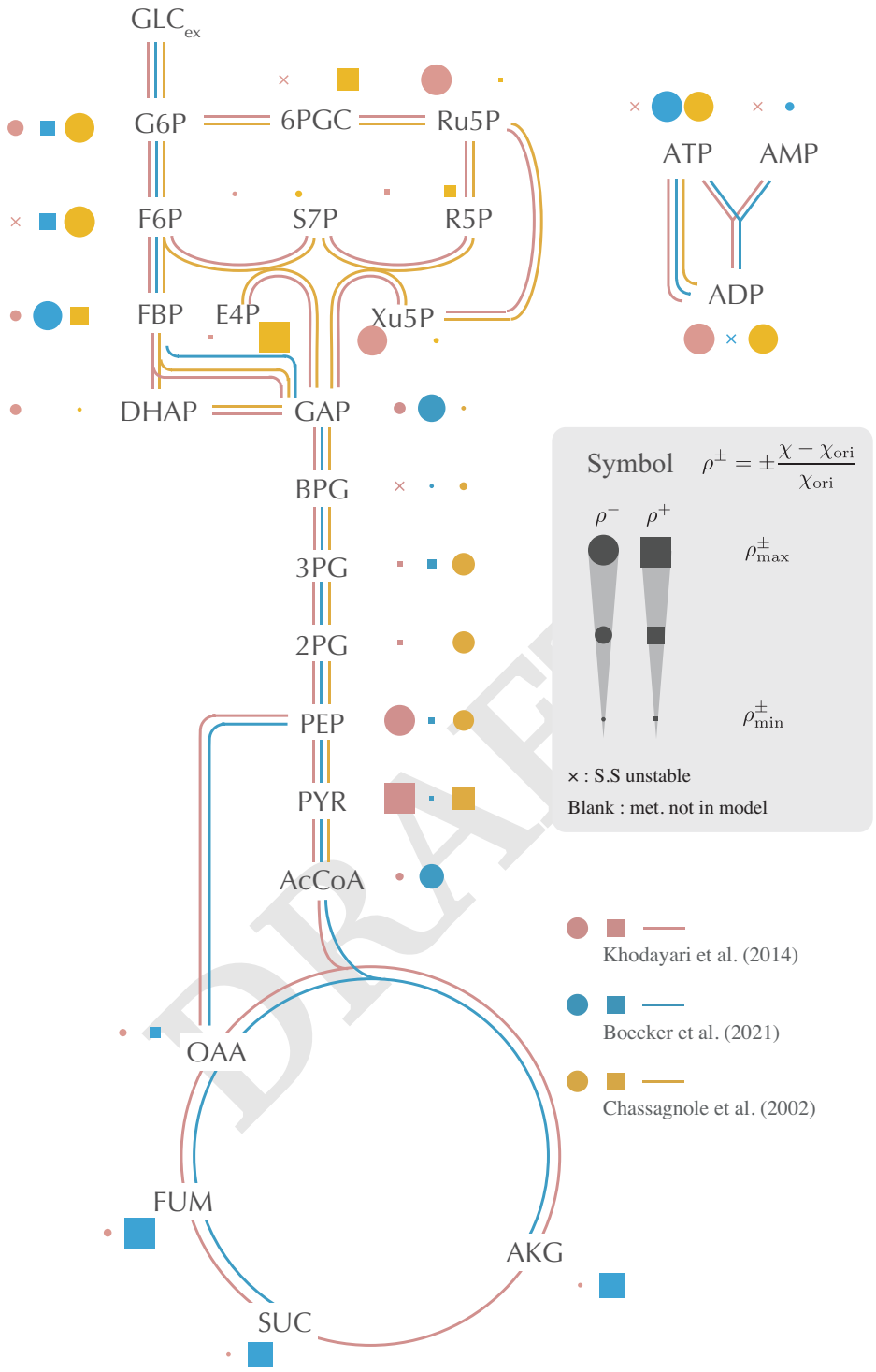

Fig. 2. The impact of setting each metabolite's concentration to its constant, steady-state value is depicted on the metabolic network. This impact is quantified by the relative change in the average response coefficient, as detailed in Eq. (1) and (2). The filled point and filled square symbols represent the decrease (ρ_x^-) and the increase (ρ_x^+) of the response coefficient, respectively. The size of the symbols is scaled using the maximum and minimum values of $\rho_x^{\pm}$ computed for each model. The cross symbol indicates that the original steady-state attractor becomes unstable when the concentration of the corresponding metabolite is fixed. If a dot, square, or cross is absent, the concentration of the corresponding metabolite is not a variable in the model. Only selected, representative metabolites are displayed in the figure. Comprehensive results are provided in Fig. S3.

works to display dynamics characterized by weak responses, we are compelled to investigate the influence of network sparseness on the dynamic behavior of metabolic models. To this end, we increase the reaction density of the metabolic network

in the three models and assess the resultant changes in responsiveness. Our approach entails initially introducing N_{add} random reactions into the network and subsequently allocating kinetic parameters to these additions from the distribution of parameter values computed from the original model. We then execute a perturbation-response simulation on this extended model to determine the response coefficient, which in turn helps ascertain the distribution and average of these coefficients. This process is schematically depicted in Fig. 3A.

Fig. 3B illustrates the alterations in responsiveness resulting from the model extensions. We generated extended metabolic networks and accompanying ODE models by adding N_{add} random reactions, and executed the perturbation-response simulation. The average response coefficient is then computed for each model and the distribution of the average response coefficient is presented as the violin plots. In the perturbation-response simulation, the extended models with only a single attractor are subjected to the response coefficient analysis (comprehensive procedural details available in the *Materials and Methods* section).

As evident from the figures, a consistent trend emerges across the three models: the introduction of random reactions weakens responsiveness. However, the magnitude of this reduction varies among the models. It is important to note that the reactants of the added reactions are selected randomly, thus not based on any specific chemical rationale. Nevertheless, this diminished responsiveness persists even when the additional reactions are confined solely to those cataloged in the metabolic model database, as visualized in Fig. S4.

Such attenuation aligns with expectations shaped by prior studies on dense reaction networks (4, 24, 28, 29). Evidently, the inherent sparsity of the backbone reaction network plays a critical role, enabling the kinetic model of metabolic systems to respond strongly to perturbations.

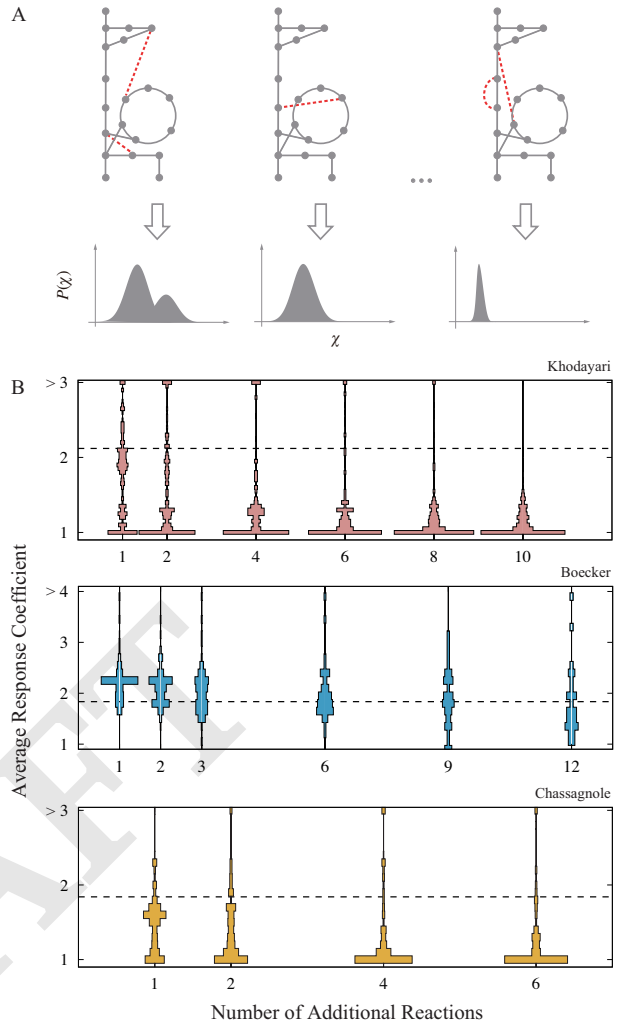

Fig. 3. (A). A schematic figure of the network expansion simulation. Reactions are randomly added to the original metabolic network, and then, the corresponding ODE model is constructed. In the illustration, the additional reaction is highlighted as the broken red lines. The perturbation response simulation is performed on the expanded models to obtain the response coefficient distribution. The average response coefficient is calculated as a scalar indicator of the responsiveness for each response coefficient distribution. (B). The distribution of the average response coefficient is plotted against the number of additional reactions for the three models. The broken line indicates the average response coefficient of the original model with no additional reaction. For each N_{add}, we generated 256 extended network, and 128 trajectories were computed for each extended network.

A minimal model for disrupted homeostasis. So far, we have studied the kinetic models of the central carbon metabolism of *E.coli*. Our findings indicate that cofactors and the sparsity of the backbone network (network devoid of cofactors) are the keys to the responsiveness of the metabolic dynamics. In this section, we develop a simple minimal model to investigate if these two factors are sufficient to induce strong responses in reaction systems.

Our minimal model is designed in a manner that allows us to adjust the sparsity of the backbone network and the proportion of cofactor-coupled reactions. First, we explain the construction of the backbone networks. These networks are comprised of N chemical species, $\mathrm{C}_1, \mathrm{C}_2, \cdots, \mathrm{C}_N$, and R reactions ($R \geq N-1$). For simplicity, we construct the backbone network using only uni-uni reactions. The minimum number of uni-uni reactions required to interlink N chemical species is $N-1$. To assemble a backbone network with N chemicals and R reactions, we first connect N reactions using $N-1$ reactions and subsequently introduce random reactions for the pairs of chemicals that lack reactions, totaling $R-(N-1)$. We incorporate exchange reactions with extracellular environments for 5% of the metabolites (this percentage is not critical to the results). The exchange reactions are always introduced to the two endpoints metabolites of the sequential linkage to ensure there are no dead-ends on reaction networks. We posit that one of the endpoint metabolites from the sequential linkage is the nutrient metabolite, and we set its external concentration at 100, while for the remainder, it is set to unity.

As cofactors, we introduce the three forms of the activation for mimicking AXP, $\mathrm{A}^{**}, \mathrm{A}^{*}$ and A, which are not included in the N chemicals in the backbone network. We introduce the coupling fraction f to modulate the number of reactions with cofactor coupling. With the coupling fraction f, the number of reactions with cofactor coupling is given as $\mathrm{Round}(fR)$ with $\mathrm{Round}(\cdot)$ as the function to round the value to the nearest integer. When a reaction is selected for cofactor coupling, two forms of the cofactor (chosen from $\mathrm{A}^{**}, \mathrm{A}^{*}$ and A) are randomly selected. The reaction then gets coupled to the conversion between these two cofactor forms, with the direction being randomly set.

Overall, the differential equation governing the minimal

DRAFT

model can be expressed as

$$\frac{\mathrm{d}x_n}{\mathrm{d}t} = \sum_{r=1}^{R} S_{nr} J_r(\boldsymbol{x}) + D_n(X_n - x_n), \qquad [3]$$

In this expression, the concentrations of the chemicals from the backbone network, as well as the cofactors, are combined in a vertical stack, i.e., $n = 1, 2, \cdots, N, N+1, N+2, N+3$. x_n with $n = 1, \cdots, N$ represents the concentrations of the nth chemical in the backbone network, and x_{N+1}, x_{N+2} and x_{N+3} denote the concentrations of $\mathrm{A}^{**}, \mathrm{A}^{*}$ and A, respectively. S is the stoichiometric matrix of the reaction network. D_n is unity if the nth chemical has an influx/efflux term, otherwise, it is zero. X_n is the external concentration of chemical n, which is a constant parameter.

Mass action kinetics is employed for the reaction rate function J_r. The rate function has the form

$$J_r(\boldsymbol{x}) = v_r \Big(k_r^{+} \prod_{n \in \mathrm{Sub}(r)} x_n - k_r^{-} \prod_{n \in \mathrm{Prd}(r)} x_n \Big) \qquad [4]$$

where $\mathrm{Sub}(r)$ and $\mathrm{Prd}(r)$ are the set of substrates and products, respectively, of the rth reaction. If the reaction is coupled with the cofactor, $|\mathrm{Sub}(r)| = |\mathrm{Prd}(r)| = 2$ and otherwise $|\mathrm{Sub}(r)| = |\mathrm{Prd}(r)| = 1$. We neither allowed the self-loops in the backbone network ($\mathrm{C}_n \rightleftharpoons \mathrm{C}_n$) nor the catalytic activity of the cofactors (e.g., $\mathrm{C}_n + \mathrm{A}^{*} \rightleftharpoons \mathrm{C}_m + \mathrm{A}^{*}$).

The parameters v_r and $k_r^{\pm}$ are the reaction rate and irreversibility, respectively. The v_r values are randomly set as $v_r = 10^{u_r}$ with the uniformly distributed random number, $u_r \sim U(-3.66, 7.13)$. The range for the kinetic parameter is derived from the Khodayari model. $k_r^{\pm}$ is calculated using the Arrhenius equation based on the standard chemical potential of each chemical. We randomly set the standard chemical potential μ_n for each chemical, where μ_n follows the uniform distribution $U(0, 1)$, while the standard chemical potentials of $\mathrm{A}^{**}, \mathrm{A}^{*}$ and A are fixed to the constant values, $1.0, 0.5$, and 0.0, respectively. To satisfy the detailed balance condition, $k_r^{\pm}$ are then given by $k_r^{\pm} = \min\{1, \exp(\mp\beta\Delta\mu_r)\}$ with $\Delta\mu_r$ as the standard chemical potential difference between the products and the substrates, $\Delta\mu_r = \sum_{n \in \mathrm{Prd(r)}} \mu_n - \sum_{n \in \mathrm{Sub}(r)} \mu_n$, and β is the inverse temperature.

We generate M networks for several choices of reaction number R and coupling fraction f. We performed the perturbation-response simulation to determine the response coefficient distribution of each network. In Fig. 4, the average response coefficient, averaged over the networks, is depicted as functions of R and f (see the rectangles labeled as "Cofactor"). These figures clearly illustrate that the average responsiveness tends to decrease as either R increases or f decreases.

The coupling with the cofactors leads to the two-body reactions, and thus, increases the nonlinearity of the model equation. It is noteworthy that the increase in responsiveness with f cannot be fully attributed to the increase in the model's nonlinearity. To validate this, we employed the model Eq. (3) without the cofactors, but incorporated catalytic reactions. In this model, each reaction proceeds with the catalytic ability of an enzyme, represented as $\mathrm{C}_n + \mathrm{C}_l \rightleftharpoons \mathrm{C}_m + \mathrm{C}_l$ (here, autocatalytic reactions are permissible, meaning l can be either n or m).

In terms of the numbers of constant, linear, and quadratic terms in the model equation, the catalytic reaction version of the model corresponds to the $f = 1$ case of the original minimal model. If the increase in responsiveness with f is dictated solely by nonlinearity, the catalytic reaction model should have comparable responsiveness with the "cofactor" model with high f. Yet, as shown in the rectangles above the main plot in Fig. 4 (labeled as "Catalytic"), the responsiveness metrics are notably lower than those observed in the minimal model.

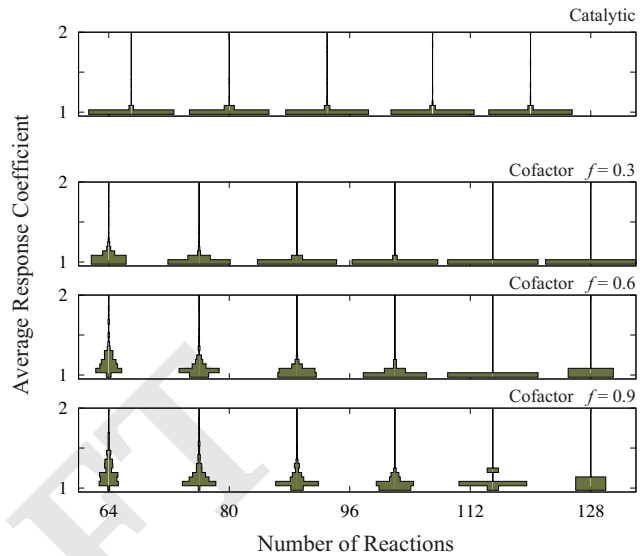

Fig. 4. The distribution of the average response coefficient is plotted against the number of reactions, R, for the model with $N = 64$ metabolites plus 3 cofactors (the panels labeled as "Cofactor") and $N = 67$ metabolites without cofactors (the panel labeled as "Catalytic"). For each combination of R and f, we generated 512 random network, and computed 128 trajectories for each of these networks. The inverse temperature β is set at 10 for the cofactor version and 20 for the catalytic version. This is because the maximum chemical potential difference in the cofactor version is 2.0, but it is 1.0 in the catalytic version. The total concentrations of the cofactors are set to be unity.

Discussion

In the present manuscript, we have studied three models of *E. coli*'s central carbon metabolism. Our findings indicate that these models commonly exhibit strong and weak responses to perturbations of the steady-state concentration. In the weak response, the effect of the perturbation dwindles almost monotonically over time. In contrast, during a strong response, initial deviations from the steady state get amplified. We introduced the response coefficient, χ, as a metric to quantify the strength of these responses and undertook comprehensive computational analyses.

We aim to identify key metabolites whose dynamics play a crucial role in the emergence of strong response. We systematically fixed the concentration of each metabolite to its steady-state value and assessed the influence of individual metabolite dynamics on the overall response strength. For a majority of metabolites, the impact on the response coefficient is bidirectional: halting the dynamic concentration of a metabolite can either amplify or diminish the response, depending upon the base model. Even if their effects consistently amplify or diminish the response, the magnitude of change in the average response coefficients remains relatively modest.

DRAFT

However, three metabolites—ATP, ADP, and pyruvate—stood out. They consistently and significantly influenced the average response coefficient across models. Pyruvate's pronounced impact can be attributed to the phosphotransferase system, whereas the effects of ATP and ADP seem to arise synergistically across multiple reactions.

One of the authors has recently reported a kinetic model of *E.coli* metabolism to exhibit anomalous relaxations and the role of AXPs in the relaxations (26). In the paper, they reduced the metabolic network into a coarse-grained minimal network. The minimal network revealed that, depending on the initial conditions, a futile cycle conversing ATP into AMP be overly active. Then, the futile cycle can deplete ATP and ADP, leading to a significant slowdown or even cessation of several ATP/ADP-coupled reactions, pushing the entire metabolic network into a "choked" state. The extensive connectivity of AXPs is a common trait in metabolic models. Hence, it is plausible that the impact of AXPs' dynamics on the entire metabolic system is a common feature irrespective of specific kinetic models.

Several experimental studies underscore the pivotal role of AXPs in metabolic homeostasis. For example, Teusink et al. demonstrated that in yeast, a sudden increase in glucose levels in the culture medium can activate a positive feedback loop in ATP production in the glycolytic pathway, leading to growth arrest (30, 31). This phenomenon of growth arrest, triggered by a nutrient level surge, has been observed across various bacterial species, including *E.coli* (32–34), though its molecular mechanism has been most extensively studied in *S. cerevisiae*. Moreover, a rapid decrease in the total adenyl cofactor concentration as a cellular response to external glucose up-shift has been documented (35–38). Walther et al. found that inhibiting this transient reduction in the adenyl cofactor pool increased the number of cells transitioning to a growth-arrested state upon glucose up-shift (38).

Next, we focused on the structure of the backbone network as suggested by the relatively simple dynamics typically observed in the random network metabolic models (4, 24, 28, 29). To this end, we increased the density of the backbone network in the three models by randomly selecting metabolites and introducing hypothetical reactions between them. The perturbation-response simulation on the extended models indicated that as more reactions were integrated, the system's response weakened.

Finally, we devised a minimal model to evaluate our hypothesis that the dynamics of cofactors and the sparsity of the backbone network are pivotal determinants of responsiveness. This model successfully showed a strong response to perturbations when the fraction of reactions to be coupled with cofactors becomes high and the backbone network is sparse. It is worth noting that the heightened response due to cofactor coupling is not solely a result of the model equation's increased nonlinearity. Interestingly, the model's catalytic reaction variant demonstrated attenuated responses to perturbations, even though its nonlinearity mirrored that of the minimal model where all reactions were cofactor-coupled.

The present study showed that there are similar metabolic responses to perturbations across three distinct kinetic models of *E.coli* metabolism. We like to underscore that these models were proposed by different research groups and within distinct contexts. Furthermore, the specifics of each model diverge considerably: both the Khodayari and Chassagnole models are tailored for aerobic conditions, whereas the Boecker model is for anaerobic conditions. Certain reactions and metabolites present in the Khodayari model are absent in both the Boecker and Chassagnole models. It goes without saying that the reaction rate functions and parameter values differ across these models. Yet, in spite of these pronounced disparities, the models exhibit converging characteristics to a certain degree, notably the pivotal role of AXPs and the diminishing responsiveness attributed to the addition of reactions. Such congruence in outcomes might hint at the presence of features that remain resilient against variations in model specifics, potentially being shaped by the foundational network structures inherent to core metabolic processes.

From a theoretical standpoint, the robustness of metabolic systems, as well as the interplay between network structure and reaction dynamics, have been explored in the chemical reaction network theory and related fields (29, 39–41). However, the practical relevance of these theories to metabolic systems remains to be ascertained since the theories are mathematically rigorous and the strong assumptions narrow down the applicable systems. The cross-talk between bacterial physiology and chemical reaction network theory should enhance the developments of each field.

In the following paragraphs, we discuss potential implications of strong responsiveness in the context of biological sciences. The unique feature of strong responsiveness, as observed in our realistic metabolic model, naturally prompts the question: what could be its biological function? An initial hypothesis suggests its role in sensing ambient condition changes and fluctuations. Well-known design principles of signal transduction systems emphasize the amplification of external stimuli (42). Given that certain transcription factors are known to sense concentrations of metabolites in central carbon metabolism (43–45), strong responsiveness could serve as an amplifier for external cues.

Additionally, this pronounced metabolic responsiveness to perturbations might play a role in the formation of spontaneous persister cells. Bacterial persistence, a phenomenon where a minor fraction of an isogenic bacterial population tolerates antibiotics despite lacking resistance genes, poses a significant challenge to therapeutic approaches (46–50). Several scenarios explain the spontaneous formation of such cells. One attributes it to the stochastic nature of gene expression dynamics, where genes triggering dormancy are activated randomly (51–53). Another scenario proposes that metabolic state fluctuations cause significant deviations from steady-state metabolite concentrations, which, when detected by cellular stress response systems, push the cell into a dormant state (14, 54). In this context, the strong metabolic responsiveness detailed in our study might be instrumental in driving cells away from a growth-centric state, prompting a transition to dormancy.

From an evolutionary standpoint, it is considered that early enzymes exhibited promiscuity, obtaining specificity over time (55–57). While specificity evolution is often linked to enhanced efficiency in vital metabolite production, our study suggests another possible outcome: improved metabolic system responsiveness. If this heightened responsiveness is adeptly integrated into gene regulatory systems, it might provide cells with an evolutionary advantage in adapting to environmental fluctuations, further enhancing the evolution of enzymatic

DRAFT

specificity.

Exploring metabolic dynamics also holds promise for synthetic biology and metabolic engineering (58–65). The construction of artificial metabolic reaction networks often relies on pathway prediction algorithms, constraint-based models, and machine learning (8, 9, 66–68). While these algorithms consider stoichiometric feasibility, they frequently overlook dynamics. This oversight can result in proposed network structures underperforming (59–62), especially in terms of cofactor recycling (64, 65). Notably, *in silico* reconstructed metabolic systems often disrupt cofactor balance (69, 70), posing challenges to bottom-up synthesis in artificial cells. We hope our study offers foundational insights for the development of quantitative metabolic dynamics theories.

Acknowledgments

The authors thank Namiko Mitarai and Taro Furubayashi for fruitful discussions. This work is supported by JSPS KAKENHI Grant Numbers JP 21K20626, JP 22K15069, and JP 22H05403 to YH; JP 22K21344 to CF; and the Japan Science and Technology Agency (JST) ERATO (JPMJER1902 to CF).

Code availability

Codes for generating the computational models studied in the manuscript are deposited on GitHub (https://github.com/yhimeoka/Perturbation-Response-Analysis.git).

Materials and Methods

Models and modifications. In Khodayari et al. (22), the kinetic parameter values are estimated by using the ensemble modeling (22, 71–73) so that the steady flux distribution of the metabolic reactions becomes consistent with the experimental measurements. However, the steady-state dealt with in the paper turned out to be unstable, i.e., the maximum eigenvalue of the Jacobi matrix of the linearized system at the steady state was positive. For carrying out the perturbation-response simulation, we need to make the steady-state stable. To make the steady-state stable, we fixed the periplasmic hydrogen concentration to the steady-state value and removed the competitive inhibition of phosphoenolpyruvate carboxylase (Those two factors were manually found). Also, we set the concentrations of the metabolites in the culture media (extracellular metabolites) with the assumption that the model cell is growing in a sufficiently large flask. In addition, the small molecules, H_2O, O_2, CO_2, NH_4 and phosphate, are set to be constant with further assuming that the exchange rate of the small chemicals between the extracellular culture is sufficiently fast.

For the dynamics of ATP and ADP concentrations, in the Chassagnole model (21), we used the reactions that coupled with ATP and ADP. Since the kinetic rate equations of those reactions are defined with the dependency of ATP and ADP concentrations in the original model, we utilized the kinetic rate equations as they are. The reactions for the adenine base synthesis are not modeled in the model, and thus, the total concentration of ATP and ADP are the conserved quantity in the model. By assuming that the decreases of the ATP and ADP due to the growth dilution are compensated, the growth dilution term is not introduced to the model equations of ATP and ADP concentrations. Lastly, we introduced the non-growth associated ATP hydrolysis reaction (ATP→ADP) since the model fails to balance ATP and ADP and relaxes to a steady state where the concentration of some metabolites is almost zero. We utilized a simple Michaelis-Menten rate equation for the hydrolysis reaction $J_{\mathrm{AH}} = v x_{\mathrm{ATP}}/(K_M + x_{\mathrm{ATP}})$, where $v = 0.1$ (sec^{-1}) and $K_M = 1.0$ (mM)

The Boecker model (23) is used without modification.

Computation of dynamics. All the ODE simulations in the present manuscript are done using `ode15s()` function in MATLAB (MathWorks) (74). For computing the attractor of the Chassagnole model, we used the initial concentrations registered in `chassagnole4` on JWS online (75) as the initial concentrations of the modified Chassagnole model to run the dynamics. The steady-state concentrations of the metabolites reach from the initial concentrations and are utilized as the attractor.

Estimate of the fluctuation strength. For estimating the strength of fluctuations, we utilize the following simple metabolic reaction

$$\emptyset \xrightarrow{P} X \xrightarrow{Q} \emptyset.$$

The concentration of the enzyme P and Q follows the stochastic transcription and translation model (76, 77). The temporal change of the concentration of the metabolite X here is given by a simple model with the mass-action kinetics,

$$\frac{\mathrm{d}x}{\mathrm{d}t} = vp(t) - uq(t)x(t), \qquad [5]$$

where x, p, q are the concentration of X, P, and Q, respectively. v and u are the kinetic parameters of the reactions. According to the time-scale separation of metabolic reactions and transcription/translation, we suppose that x is the fast variable and its dynamics slave to p and q. We assume that the timescales in the change of the metabolite concentrations are sufficiently smaller than that of the proteins and apply the quasi-steady-state approximation: we solve the steady-state of the deterministic equation of Eq. (5) (78, 79). Then, we calculate the mean and variance of the solution $x(t) = vp(t)/uq(t)$, which is a stochastic variable. Since the stochastic transcription and translation model leads to the Gamma distribution of the protein concentration, the average and the variance are given by

$$\begin{aligned}\langle x\rangle &= \frac{v/u}{b^{2a}\Gamma^2(a)}\int_{\mathbb{R}_+^2} dpdq\frac{p}{q}p^{a-1}e^{-p/b}q^{a-1}e^{-q/b} \\ &= \frac{v}{u}\frac{a}{a-1} \qquad [6]\\ \langle x^2\rangle &= \frac{v^2/u^2}{b^{2a}\Gamma^2(a)}\int_{\mathbb{R}_+^2} dpdq\frac{p^2}{q^2}p^{a-1}e^{-p/b}q^{a-1}e^{-q/b} \\ &= \frac{v^2}{u^2}\frac{a(a+1)}{(a-1)(a-2)}, \qquad [7]\end{aligned}$$

where a and b are the parameters set by the rate of the transcription, translation, mRNA degradation, and protein degradation.

The coefficient of variation is then given by

$$\frac{\sqrt{\langle x^2\rangle - \langle x\rangle^2}}{\langle x\rangle} = \sqrt{\frac{2a-1}{a(a-2)}}. \qquad [8]$$

DRAFT

a is the ratio between the transcription rate and the protein degradation rate. According to the large-scale proteomic analysis of *E.coli* (80), the mean value of a among the essential genes is $\approx 6.82 \pm 2.34$ (only with the essential metabolic enzymes listed in the iML1515 (81), the average value is $\approx 6.72 \pm 2.34$). By substituting $a = 6.82$ into Eq. (8), we obtain the relative noise strength as $\approx 62\%$. Since in the estimate, we suppose the irreversible reactions lead to larger noise amplitudes than reversible reactions, we regard 62% as the maximum relative noise strength and use a bit smaller value, 40%.

before applying the elementary reaction decomposition

The random catalytic reaction network model. The random catalytic reaction network (RCRN) model is a simple toy model of cellular metabolism (4, 24). The ordinary differential equation dictating the temporal evolution of the ith metabolite's concentration x_i is given by

$$\frac{\mathrm{d}x_i}{\mathrm{d}t} = \sum_{j,k} x_k \Big(v_{ijk} x_j - v_{jik} x_i \Big) + D_i x_{T(i)} X_i - \mu x_i,$$

where v_{ijk}, D_i and μ are the rate constant of the reaction $\mathrm{C}_j \to \mathrm{C}_i$ catalyzed by C_k (C_i denotes the ith metabolite), the substrate update rate of C_i, and the specific growth rate of the model cell, respectively. $T(i)$ denotes the transporter metabolite (enzyme) for the uptake of C_i, and X_i is the external concentration of C_i. In the RCRN model, the total volume of the cell is usually set to be equal to the total amount of the metabolites. This is because each "metabolite" in the model is interpreted as an enzyme as well as a reactant of the metabolic reactions. Hence, the specific growth rate of the model cell is set to the total uptake rate of the metabolites, $\mu = \sum_i D_i x_{T(i)} X_i$.

In the construction of an instance of the RCRN model, we first generate a random, connected network among N metabolites, and then, we assign a single catalyst on each reaction edge. If the reaction $\mathrm{C}_j \to \mathrm{C}_i$ catalyzed by C_k exists in the network, v_{ijk} is non-zero, while otherwise, it is set to zero. In the present manuscript, we suppose all the reactions are reversible, and thus, v_{jik} is non-zero if and only if v_{ijk} is non-zero.

For making the comparison of the responsiveness of the realistic model to the RCRN model, we generated 128 instances of the RCRN model where the number of metabolites N is set to be equal to the realistic model that we want to make a comparison. The number of reactions R is set to $3.5N$ for the Boecker and Chassagnole model while $4N$ for the Khodayari model. The ratio between N and R is set so that the Erdős–Rényi random graph of given size becomes connected with sufficiently high probability. The reaction rate constants v_{ijk}'s are sampled from the model to compare. For the sake of simplicity, we suppose only the 1st metabolite is the nutrient metabolite which is taken up from the external environment and the Nth metabolite is the transporter of it. D_i and X_i are set to unity for $i = 1$, and for the else, those parameters are set to zero.

For each generated instance of the RCRN model, we performed the perturbation response simulation where the attractor(s) are computed by simulating the model dynamics from randomly generated 32 initial concentrations $\boldsymbol{x}_{\mathrm{ini}} \in (10^{-3}, 10^{3})^N$. The RCRN models exhibiting multistability or computational failure due to numerical issues such as heavy stiffness are not subjected to further analysis. For quantifying the response coefficient, we computed 128 trajectories for each of those models.

Random addition of the metabolic reactions. We have added only uni-uni reactions of non-cofactor metabolites. The additional reaction is coupled to the AXPs with the probability given by the fraction of native reactions coupled to AXPs. The non-cofactor metabolites are randomly chosen from the metabolites list. Thus, the addition reaction is either the uni-uni reaction (if the reaction is not coupled with AXPs) or the bi-bi reaction (if the reaction is coupled with AXPs). We computed the parameter value distribution for each reaction scheme and the parameter values for the additional reactions are sampled from the corresponding parameter value distribution.

For the Khodayari model, the additional reaction is modeled using the elementary reaction decomposition (see the next section), i.e, a reaction $A \rightleftharpoons B$ is decomposed into the three elementary reaction steps, $E + A \rightleftharpoons EA$, $EA \rightleftharpoons EB$, and $EB \rightleftharpoons E + B$. The mass-action kinetics is adopted as the reaction rate function for each elementary reaction step.

The elementary reaction decomposition is not applied to the Boecker model and the Chassagnole model. Also, several types of reaction rate functions are used in the two models. Thus, we decided to use the simplest enzymatic reaction kinetics used in each paper. The reversible Michaelis-Menten kinetics

$$v = \frac{v_{\max}([S_1] - [P_1]/L_{\mathrm{eq}})}{1 + [S_1]/K_{S_1} + [P_1]/K_{P_1}}$$

is used for uni-uni reactions, and for bi-bi reactions, the ordered bi-bi reaction kinetics

$$v = \frac{v_{\max}([S_1][S_2] - [P_1][P_2]/L_{\mathrm{eq}})}{1 + \frac{[S_1]}{K_{S_1}} + \frac{[P_1]}{K_{P_1}} + \frac{[S_1][S_2]}{K_{S_1}K_{S_2}} + \frac{[P_1][P_2]}{K_{P_1}K_{P_2}}}$$

is adopted in the Boecker model, a reaction kinetics

$$v = \frac{v_{\max}([S_1][S_2] - [P_1][P_2]/L_{\mathrm{eq}})}{(1 + [S_1]/K_{S_1} + [P_1]/K_{P_1})(1 + [S_2]/K_{S_2} + [P_2]/K_{P_2})}$$

is used in the Chassagnole model. $[S_i], [P_i]$, L_{eq} and K_* represent the concentration of the ith substrate and product, the equilibrium constant of the reaction, and the dissociation constant of the corresponding chemical, respectively.

After constructing an extended model, we compute the steady-state attractor by simulating the dynamics from 128 initial concentrations. These are generated by applying a 40% relative perturbation to the steady-state concentrations of the original model. If all the initial conditions converge to a single attractor, then 128 initial conditions are generated by applying a 40% relative perturbation to the steady-state concentrations of the extended model in order to perform the perturbation-response simulation. For the Boecker model, we require the extended model to have a steady growth rate greater than half of that of the original model. This is because growth dilution is typically the slowest process in the model, and thus, a significant slowdown of growth dilution can lead to an artificial overestimation of the model's responsiveness.

DRAFT

Elementary reaction decomposition. Here, a brief description of the elementary reaction decomposition (ERD) is provided. Suppose that we have the following bi-to-uni reaction

$$\mathrm{A} + \mathrm{B} \rightleftharpoons \mathrm{C}, \qquad [9]$$

and that the reaction is catalyzed by an enzyme E. For implementing this reaction into the kinetic model, the Michaelis-Menten type kinetics of chemical reaction is often adopted. With the Michaelis-Menten type kinetics, the rate of the reaction J is given by

$$J = v[E]\frac{k_+[A][B] - k_-[C]}{1 + [A]/K_A + [A][B]/K_{AB} + [C]/K_C}, \qquad [10]$$

where we supposed that the binding of the substrate to the enzyme occurs in the order of $A \to B$.

The Michaelis-Meneten type reaction kinetics (Eq. (10)) is obtained by the pseudo-equilibrium approximation or the steady-state approximation of the following reactions

$$\mathrm{A} + \mathrm{E} \rightleftharpoons \mathrm{EA} \qquad [11]$$
$$\mathrm{EA} + \mathrm{B} \rightleftharpoons \mathrm{EAB} \qquad [12]$$
$$\mathrm{EAB} \rightleftharpoons \mathrm{EC} \qquad [13]$$
$$\mathrm{EC} \rightleftharpoons \mathrm{E} + \mathrm{C} \qquad [14]$$

In the ERD scheme, each step (Eq. (11)-(14)) of the overall reaction (Eq. (9)) is modeled using the mass-action kinetics. Also, the forward- and the backward reactions are dealt as different reactions. For instance, the rates of the reaction $\mathrm{A} + \mathrm{E} \rightleftharpoons \mathrm{EA}$ is given by $J_{A,E\to EA} = v_{A,E\to EA}[E][A]$ and $J_{EA\to A,E} = v_{EA\to A,E}[EA]$.

The advantage of the ERD is that every reaction rate function is given either by a linear or quadratic function of the metabolites' concentrations. This feature allows us, in the present manuscript, to randomize the reaction network in a unified manner. Also, the ERD has the advantage of reducing the computational cost for the parameter estimation based on omics data. For more details, see original papers (22, 71–73).

The generative AIs and other software. ChatGPT (OpenAI, September 25, 2023 version) and Grammarly (Grammarly, Inc.) are used to improve clarity and to brush up on English grammar.

1. M Schaechter, O Maaløe, NO Kjeldgaard, Dependency on medium and temperature of cell size and chemical composition during balanced growth of salmonella typhimurium. *Microbiology* **19**, 592–606 (1958).
2. M Scott, CW Gunderson, EM Mateescu, Z Zhang, T Hwa, Interdependence of cell growth and gene expression: origins and consequences. *Science* **330**, 1099–1102 (2010).
3. S Pirt, The maintenance energy of bacteria in growing cultures. *Proc. Royal Soc. London. Ser. B. Biol. Sci.* **163**, 224–231 (1965).
4. K Kaneko, C Furusawa, T Yomo, Universal relationship in gene-expression changes for cells in steady-growth state. *Phys. Rev. X* **5**, 011014 (2015).
5. A Roy, D Goberman, R Pugatch, A unifying autocatalytic network-based framework for bacterial growth laws. *Proc. Natl. Acad. Sci. U. S. A.* **118** (2021).
6. M Scott, T Hwa, Shaping bacterial gene expression by physiological and proteome allocation constraints. *Nat. Rev. Microbiol.* **21**, 327–342 (2023).
7. S Jun, F Si, R Pugatch, M Scott, Fundamental principles in bacterial physiology—history, recent progress, and the future with focus on cell size control: a review. *Rep. Prog. Phys.* **81**, 056601 (2018).
8. A Varma, BO Palsson, Metabolic capabilities of escherichia coli: I. synthesis of biosynthetic precursors and cofactors. *J. theoretical biology* **165**, 477–502 (1993).
9. JD Orth, I Thiele, BØ Palsson, What is flux balance analysis? *Nat. biotechnology* **28**, 245–248 (2010).
10. Y Kaplan, et al., Observation of universal ageing dynamics in antibiotic persistence. *Nature* **600**, 290–294 (2021).
11. Y Himeoka, K Kaneko, Theory for transitions between exponential and stationary phases: universal laws for lag time. *Phys. Rev. X* **7**, 021049 (2017).
12. I Levin-Reisman, et al., Automated imaging with scanlag reveals previously undetectable bacterial growth phenotypes. *Nat. Methods* **7**, 737 (2010).
13. Y Himeoka, B Gummesson, MA Sørensen, SL Svenningsen, N Mitarai, Distinct survival, growth lag, and rRNA degradation kinetics during Long-Term starvation for carbon or phosphate. *mSphere* **7**, e0100621 (2022).
14. JL Radzikowski, et al., Bacterial persistence is an active σs stress response to metabolic flux limitation. *Mol. systems biology* **12**, 882 (2016).
15. K Sekar, et al., Bacterial glycogen provides Short-Term benefits in changing environments. *Appl. Environ. Microbiol.* **86** (2020).
16. M Basan, et al., A universal trade-off between growth and lag in fluctuating environments. *Nature* **584**, 470–474 (2020).
17. E Biselli, SJ Schink, U Gerland, Slower growth of escherichia coli leads to longer survival in carbon starvation due to a decrease in the maintenance rate. *Mol. Syst. Biol.* **16**, e9478 (2020).
18. J Monod, The growth of bacterial cultures. *Annu. review microbiology* **3**, 371–394 (1949).
19. SH Strogatz, *Nonlinear dynamics and chaos with student solutions manual: With applications to physics, biology, chemistry, and engineering.* (CRC press), (2018).
20. G Nicolis, I Prigogine, *Self-Organization in Nonequilibrium Systems: From Dissipative Structures to Order Through Fluctuations*, A Wiley-Interscience publication. (Wiley), (1977).
21. C Chassagnole, N Noisommit-Rizzi, JW Schmid, K Mauch, M Reuss, Dynamic modeling of the central carbon metabolism of escherichia coli. *Biotechnol. bioengineering* **79**, 53–73 (2002).
22. A Khodayari, AR Zomorrodi, JC Liao, CD Maranas, A kinetic model of escherichia coli core metabolism satisfying multiple sets of mutant flux data. *Metab. engineering* **25**, 50–62 (2014).
23. S Boecker, et al., Deciphering the physiological response of escherichia coli under high ATP demand. *Mol. Syst. Biol.* **17**, e10504 (2021).
24. C Furusawa, K Kaneko, Zipf's law in gene expression. *Phys. review letters* **90**, 088102 (2003).
25. C Furusawa, K Kaneko, Adaptation to optimal cell growth through self-organized criticality. *Phys. Rev. Lett.* **108**, 208103 (2012).
26. Y Himeoka, N Mitarai, Emergence of growth and dormancy from a kinetic model of the escherichia coli central carbon metabolism. *Phys. Rev. Res.* **4**, 043223 (2022).
27. Y Kondo, K Kaneko, Growth states of catalytic reaction networks exhibiting energy metabolism. *Phys. Rev. E* **84**, 011927 (2011).
28. A Awazu, K Kaneko, Ubiquitous "glassy" relaxation in catalytic reaction networks. *Phys. Rev. E* **80**, 041931 (2009).
29. Y Himeoka, JB Kirkegaard, N Mitarai, S Krishna, Structural determinants of relaxation dynamics in chemical reaction networks. (2022).
30. JH van Heerden, et al., Lost in transition: start-up of glycolysis yields subpopulations of nongrowing cells. *Science* **343**, 1245114 (2014).
31. B Teusink, MC Walsh, K van Dam, HV Westerhoff, The danger of metabolic pathways with turbo design. *Trends Biochem. Sci.* **23**, 162–169 (1998).
32. RE Strange, JR Hunter, Substrate-accelerated death' of nitrogen-limited bacteria. *J. Gen. Microbiol.* **44**, 255–262 (1966).
33. JR Postgate, JR Hunter, Accelerated death of aerobacter aerogenes starved in the presence of growth-limiting substrates. *J. Gen. Microbiol.* **34**, 459–473 (1964).
34. PH Calcott, JR Postgate, On substrate-accelerated death in klebsiella aerogenes. *J. Gen. Microbiol.* **70**, 115–122 (1972).
35. U Theobald, W Mailinger, M Baltes, M Rizzi, M Reuss, In vivo analysis of metabolic dynamics in saccharomyces cerevisiae : I. experimental observations. *Biotechnol. Bioeng.* **55**, 305–316 (1997).
36. MTAP Kresnowati, et al., When transcriptome meets metabolome: fast cellular responses of yeast to sudden relief of glucose limitation. *Mol. Syst. Biol.* **2**, 49 (2006).
37. M Rizzi, M Baltes, U Theobald, M Reuss, In vivo analysis of metabolic dynamics in saccharomyces cerevisiae: II. mathematical model. *Biotechnol. Bioeng.* **55**, 592–608 (1997).
38. T Walther, et al., Control of ATP homeostasis during the respiro-fermentative transition in yeast. *Mol. Syst. Biol.* **6**, 344 (2010).
39. M Feinberg, *Foundations of Chemical Reaction Network Theory.* (Springer, Cham), (2019).
40. RN Gutenkunst, et al., Universally sloppy parameter sensitivities in systems biology models. *PLoS Comput. Biol.* **3**, 1871–1878 (2007).
41. TJ Kobayashi, D Loutchko, A Kamimura, S Horiguchi, Y Sughiyama, Information geometry of dynamics on graphs and hypergraphs. *arXiv preprint arXiv:2211.14455* (2022).
42. JE Ferrell, SH Ha, Ultrasensitivity part i: Michaelian responses and zero-order ultrasensitivity. *Trends biochemical sciences* **39**, 496–503 (2014).
43. O Kotte, JB Zaugg, M Heinemann, Bacterial adaptation through distributed sensing of metabolic fluxes. *Mol. systems biology* **6**, 355 (2010).
44. H Okano, R Hermsen, K Kochanowski, T Hwa, Regulation underlying hierarchical and simultaneous utilization of carbon substrates by flux sensors in escherichia coli. *Nat. Microbiol.* **5**, 206–215 (2019).
45. K Kochanowski, et al., Functioning of a metabolic flux sensor in escherichia coli. *Proc. Natl. Acad. Sci. U. S. A.* **110**, 1130–1135 (2013).
46. E Kussell, R Kishony, NQ Balaban, S Leibler, Bacterial persistence: a model of survival in changing environments. *Genetics* **169**, 1807–1814 (2005).
47. NQ Balaban, J Merrin, R Chait, L Kowalik, S Leibler, Bacterial persistence as a phenotypic switch. *Science* **305**, 1622–1625 (2004).
48. NQ Balaban, et al., Definitions and guidelines for research on antibiotic persistence. *Nat. Rev. Microbiol.* **17**, 441–448 (2019).
49. M Umetani, et al., Observation of non-dormant persister cells reveals diverse modes of survival in antibiotic persistence. (2021).
50. Y Wakamoto, et al., Dynamic persistence of antibiotic-stressed mycobacteria. *Science* **339**, 91–95 (2013).
51. S Ronneau, S Helaine, Clarifying the link between Toxin-Antitoxin modules and bacterial persistence. *J. Mol. Biol.* **431**, 3462–3471 (2019).
52. A Harms, DE Brodersen, N Mitarai, K Gerdes, Toxins, targets, and triggers: An overview of Toxin-Antitoxin biology. *Mol. Cell* **70**, 768–784 (2018).
53. A Harms, C Fino, MA Sørensen, S Semsey, K Gerdes, Prophages and growth dynamics

DRAFT

confound experimental results with Antibiotic-Tolerant persister cells. *MBio* **8** (2017).
54. JL Radzikowski, H Schramke, M Heinemann, Bacterial persistence from a system-level perspective. *Curr. Opin. Biotechnol.* **46**, 98–105 (2017).
55. O Khersonsky, DS Tawfik, Enzyme promiscuity: a mechanistic and evolutionary perspective. *Annu. Rev. Biochem.* **79**, 471–505 (2010).
56. H Innan, F Kondrashov, The evolution of gene duplications: classifying and distinguishing between models. *Nat. Rev. Genet.* **11**, 97–108 (2010).
57. RA Jensen, Enzyme recruitment in evolution of new function. *Annu. Rev. Microbiol.* **30**, 409–425 (1976).
58. Y Shimizu, et al., Cell-free translation reconstituted with purified components. *Nat. Biotechnol.* **19**, 751–755 (2001).
59. T Schwander, L Schada von Borzyskowski, S Burgener, NS Cortina, TJ Erb, A synthetic pathway for the fixation of carbon dioxide in vitro. *Science* **354**, 900–904 (2016).
60. A Bar-Even, E Noor, NE Lewis, R Milo, Design and analysis of synthetic carbon fixation pathways. *Proc. Natl. Acad. Sci. U. S. A.* **107**, 8889–8894 (2010).
61. A Doerr, et al., Modelling cell-free RNA and protein synthesis with minimal systems. *Phys. Biol.* **16**, 025001 (2019).
62. NJ Claassens, S Burgener, B Vögeli, TJ Erb, A Bar-Even, A critical comparison of cellular and cell-free bioproduction systems. *Curr. Opin. Biotechnol.* **60**, 221–229 (2019).
63. M Kurisu, et al., Synthesising a minimal cell with artificial metabolic pathways. *Commun. Chem.* **6**, 1–14 (2023).
64. PH Opgenorth, TP Korman, L Iancu, JU Bowie, A molecular rheostat maintains ATP levels to drive a synthetic biochemistry system. *Nat. Chem. Biol.* **13**, 938–942 (2017).
65. PH Opgenorth, TP Korman, JU Bowie, A synthetic biochemistry molecular purge valve module that maintains redox balance. *Nat. Commun.* **5**, 4113 (2014).
66. Y Moriya, et al., PathPred: an enzyme-catalyzed metabolic pathway prediction server. *Nucleic Acids Res.* **38**, W138–43 (2010).
67. M Araki, et al., M-path: a compass for navigating potential metabolic pathways. *Bioinformatics* **31**, 905–911 (2015).
68. MHS Segler, M Preuss, MP Waller, Planning chemical syntheses with deep neural networks and symbolic AI. *Nature* **555**, 604–610 (2018).
69. M Okamoto, A Katsurayama, M Tsukiji, Y Aso, K Hayashi, Dynamic behavior of enzymatic system realizing two-factor model. *J. Theor. Biol.* **83**, 1–16 (1980).
70. M Okamoto, K Hayashi, Dynamic behavior of cyclic enzyme systems. *J. Theor. Biol.* **104**, 591–598 (1983).
71. LM Tran, ML Rizk, JC Liao, Ensemble modeling of metabolic networks. *Biophys. journal* **95**, 5606–5617 (2008).
72. Y Tan, JC Liao, Metabolic ensemble modeling for strain engineers. *Biotechnol. journal* **7**, 343–353 (2012).
73. ML Rizk, JC Liao, Ensemble modeling for aromatic production in escherichia coli. *PloS one* **4**, e6903 (2009).
74. TM Inc., Matlab version: 9.12.0 (r2022a) (2022).
75. BG Olivier, JL Snoep, Web-based kinetic modelling using jws online. *Bioinformatics* **20**, 2143–2144 (2004).
76. N Friedman, L Cai, XS Xie, Linking stochastic dynamics to population distribution: an analytical framework of gene expression. *Phys. Rev. Lett.* **97**, 168302 (2006).
77. J Paulsson, M Ehrenberg, Random signal fluctuations can reduce random fluctuations in regulated components of chemical regulatory networks. *Phys. Rev. Lett.* **84**, 5447–5450 (2000).
78. K Kaneko, Adiabatic elimination by the eigenfunction expansion method. *Prog. Theor. Phys.* **66**, 129–142 (1981).
79. H Risken, Fokker-Planck equation in *The Fokker-Planck Equation: Methods of Solution and Applications*, ed. H Risken. (Springer Berlin Heidelberg, Berlin, Heidelberg), pp. 63–95 (1996).
80. Y Taniguchi, et al., Quantifying e. coli proteome and transcriptome with single-molecule sensitivity in single cells. *Science* **329**, 533–538 (2010).
81. JM Monk, et al., i ml1515, a knowledgebase that computes escherichia coli traits. *Nat. biotechnology* **35**, 904–908 (2017).

DRAFT

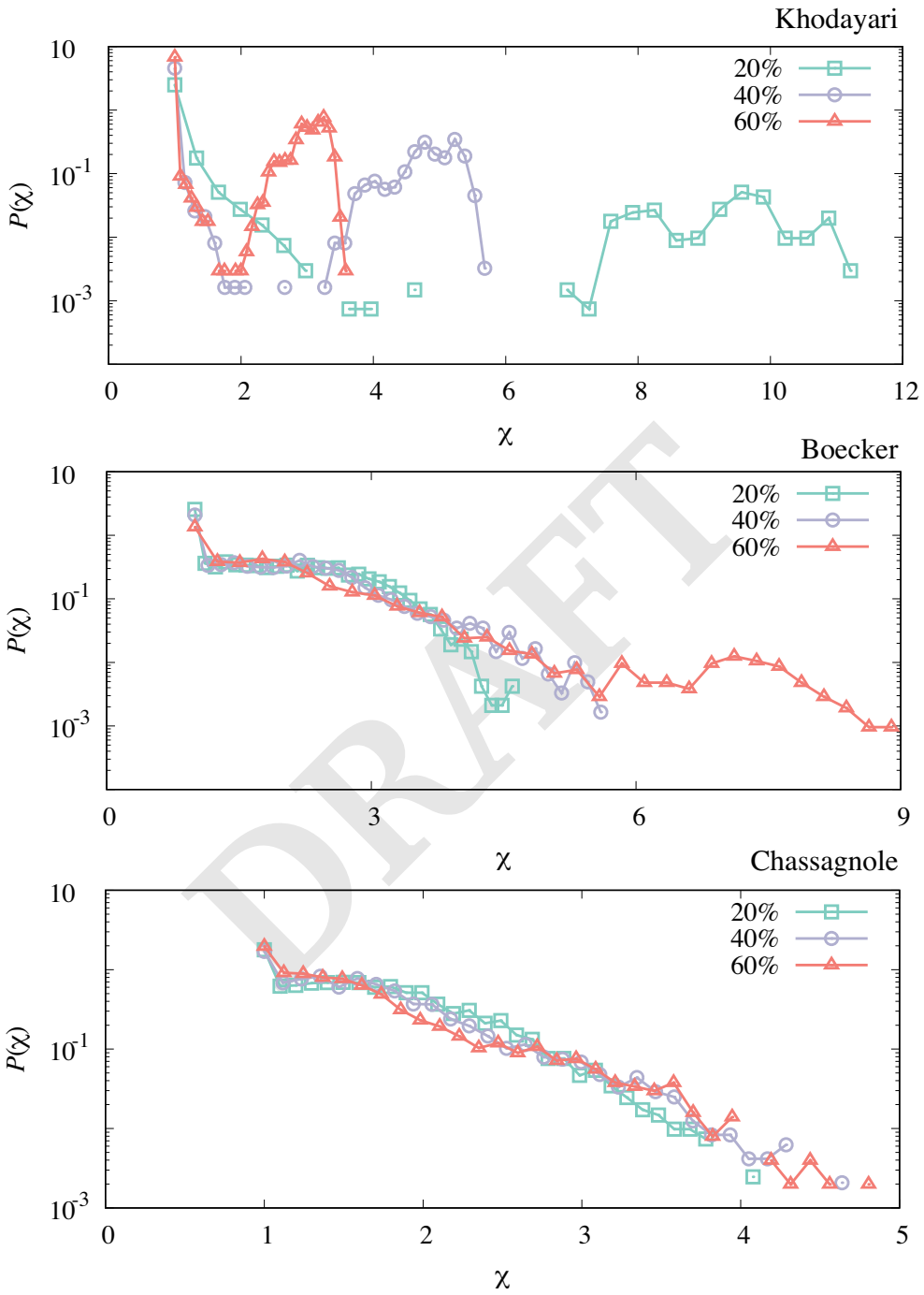

Fig. S1. The response coefficient distribution of each model obtained by the perturbation-response simulation with different perturbation strengths ($20\%, 40\%$ and 60% relative perturbation). Each distribution is obtained by simulating 4096 trajectories. The qualitative features (double-peaks for the Khodayari model and the plateau for the Boecker and Chassagnole models) are unvaried, while the scales of the response coefficient of the Khodayari model differ among the perturbation strengths.

DRAFT

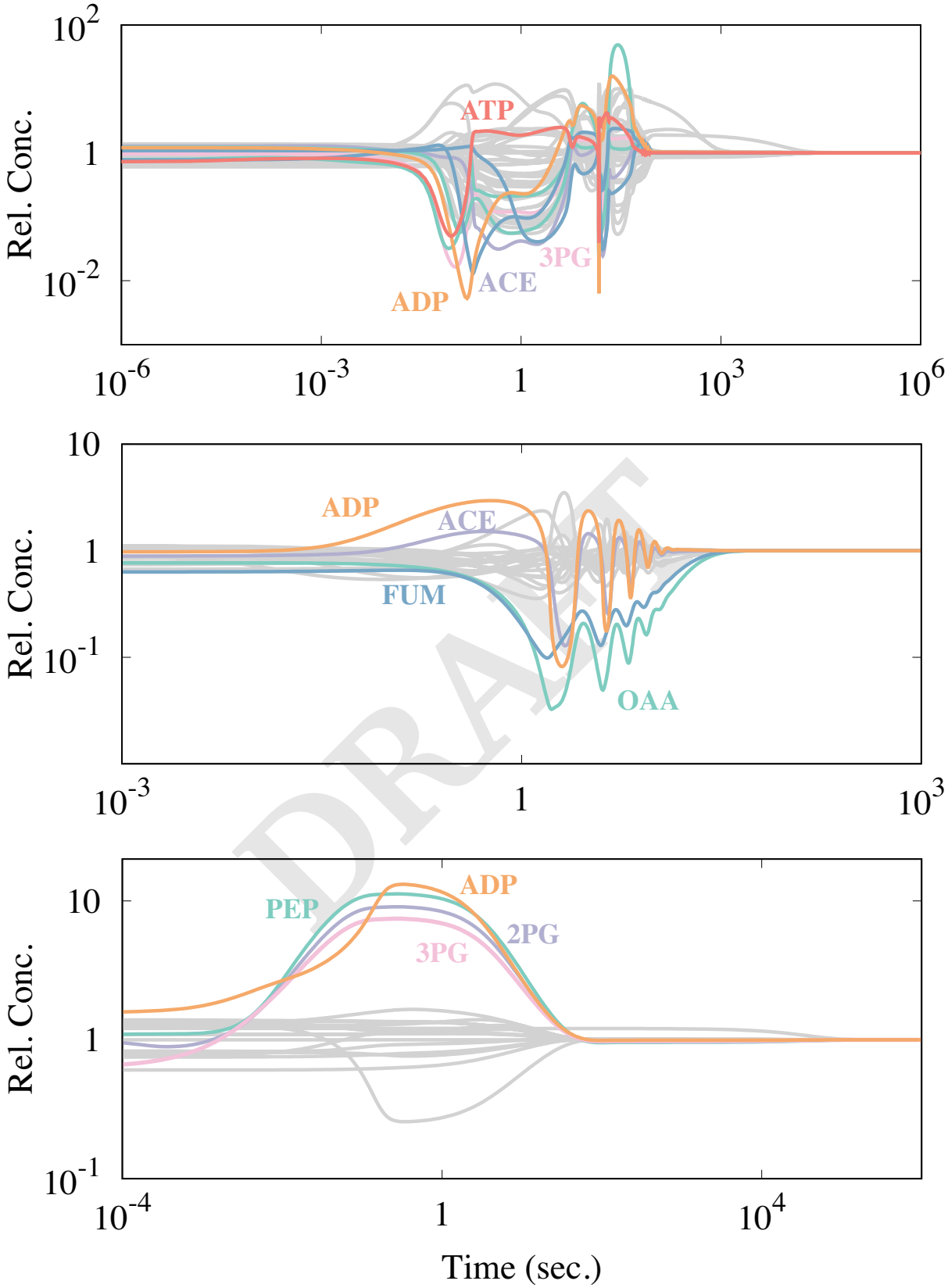

Fig. S2. The time course of each model with the strongly responding metabolites being highlighted. A metabolite is highlighted if its concentration changes more than X-fold from its steady concentration. X is set to be 5 for the Boecker and Chassagnole models, while $X = 25$ is chosen for the Khodayari model because too many metabolites are highlighted with $X = 5$.

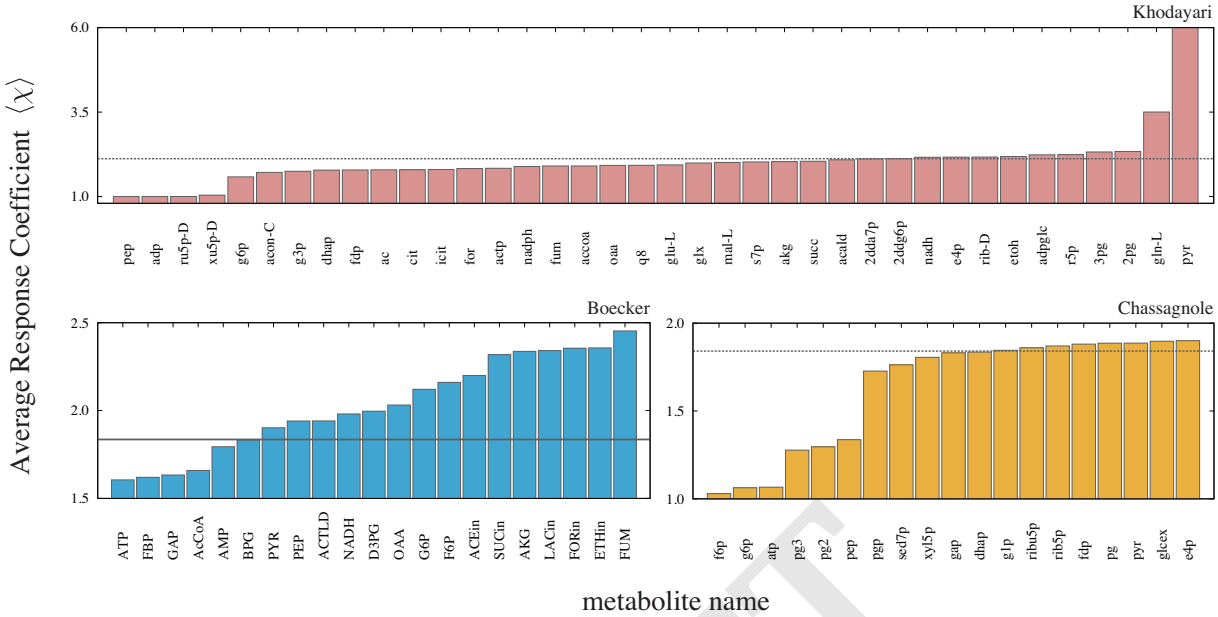

Fig. S3. The average response coefficients of the models with the concentration of indicated metabolite fixed. The dashed line in each panel is the average response coefficient of the original model.

DRAFT

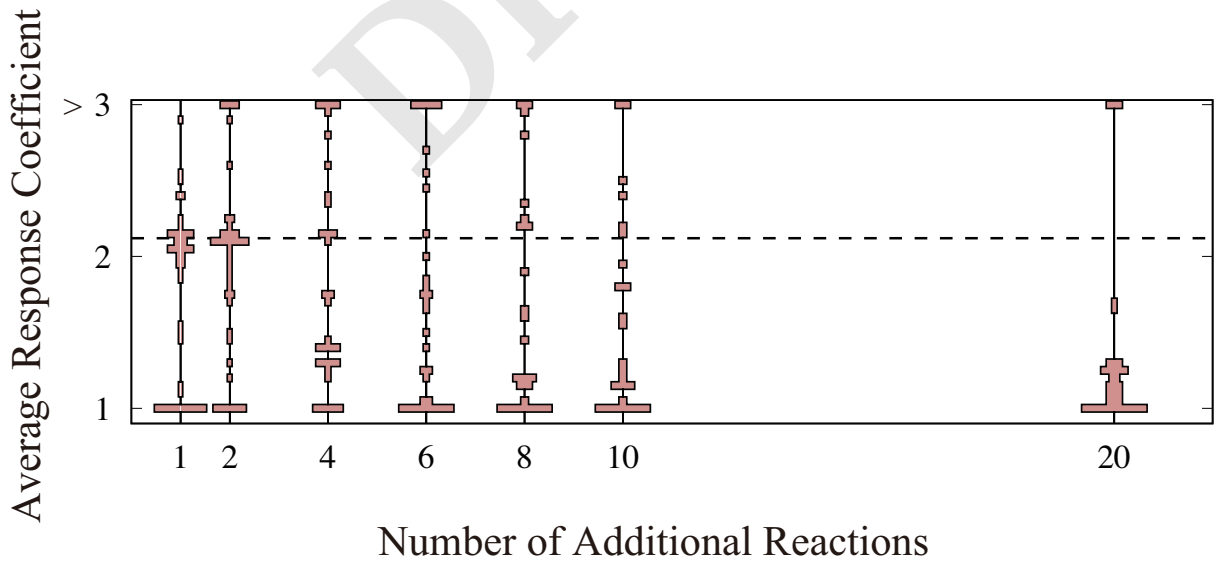

Fig. S4. The violin plot of the average response coefficient of the network expansion of the Khodayari model. The horizontal axis represents the number of additional reactions. The additional reactions are chosen from the reactions registered in the metabolic model database (see Table. S1).

Table S1. The list of the additional reactions used for generating Fig. S4.

Reaction ID	Substrates	Products	BiGG Model ID
CITL	cit_c	ac_c, oaa_c	iYS1720
NADPHQR2	nadph_c, q8_c	nadp_c, q8h2_c	iYS1720
OAADC	oaa_c	pyr_c	iYS1720
POX	pyr_c, q8_c	ac_c, q8h2_c	iYS1720
ALDD2y	acald_c, nadp_c	ac_c, nadph_c	iYS1720
FDH	for_c, nad_c	nadh_c	iYO844
ACONT	cit_c	icit_c	iYO844
ALCD2y	etoh_c, nadp_c	acald_c, nadph_c	iYO844
GAPDi_nadp	13dpg_c, nadph_c	g3p_c, nadp_c	iYO844
ALDD2x	acald_c, nad_c	ac_c, nadh_c	iYO844
ACYP_2	actp_c	ac_c	iSB619
FRDx	fum_c, nadh_c	nad_c, succ_c	iNF517
ICDHxm	icit_c, nad_c	akg_c, nadh_c	iMM904
PYRDC	pyr_c	acald_c	iMM904
ACYP	13dpg_c	3pg_c	iMM1415
ADPGLC	adpglc_c	amp_c, g1p_c	iMM1415
ETOHMO	etoh_c, nadph_c	acald_c, nadp_c	iMM1415
PKETF	f6p_c	actp_c, e4p_c	iLB1027_lipid
G6PDH1	g6p_c, nad_c	6pgl_c, nadh_c	iIT341
ASCTmr	accoa_c, succ_c	ac_c, succoa_c	iIS312
PGAM1_PhosHydro	pep_c	pyr_c	iCHOv1
PFK_adp	adp_c, f6p_c	amp_c, fdp_c	iAF692

DRAFT